Appl. Phys. B (2016) 122:10
DOI 10.1007/s00340-015-6294-7

Applied Physics B
Lasers and Optics

Quantum cascade laser-based sensors for the detection of exhaled carbon monoxide

Nahid Pakmanesh[1,2] · Simona M. Cristescu[2] · Atamalek Ghorbanzadeh[1] · Frans J. M. Harren[2] · Julien Mandon[2]

Received: 14 April 2015 / Accepted: 23 November 2015 / Published online: 20 January 2016

Abstract Carbon monoxide (CO) is an important biomarker as it originates in the human body from the heme (component of hemoglobin) degradation. Tunable laser absorption spectroscopy in the mid-infrared wavelength region is used for sensitive trace gas sensing of exhaled carbon monoxide (CO). Based on a quantum cascade laser emitting at 4.61 μm, two different spectroscopic methods are investigated: off-axis integrated cavity output spectroscopy (OA-ICOS) and wavelength modulation 2f/1f spectroscopy (WMS). The optical sensors integrate a slow feedback system to correct for wavelength drifts improving their stability over days. Both approaches demonstrate a high reproducibility and sensitivity during online measurements of exhaled human breath. Considering the detection limit to be the equal to the standard deviation of the background fluctuations, the noise-equivalent detection limit for both OA-ICOS and WMS is 7 ppbv (1-s averaging time), leading to a noise-equivalent absorption sensitivity of 3.1×10^{-7} cm^{-1} Hz$^{-1/2}$, which is sufficient for measurements of exhaled CO (eCO). Collection and measurements of eCO samples were investigated, and different exhalation flow rates and breath-holding time were explored, to provide a reliable sampling method for future medical investigations.

✉ Julien Mandon
j.mandon@science.ru.nl

[1] Department of Physics, University of Tehran, North Kargar St., Tehran 1439955961, Iran

[2] Department of Molecular and Laser Physics, Radboud University Nijmegen, Nijmegen, The Netherlands

1 Introduction

The sampling of biomarkers in exhaled breath is of interest for the clinical practice, because of its noninvasive character as compared to other sampling methods. Among the hundreds of molecules released in human breath, one of the important endogenously produced inorganic gases is carbon monoxide (CO). Almost 80 % of CO in the human body is produced by catalytic breakdown of heme by the microsomal heme oxygenase (HO) enzyme [1–3]. Most of the formed CO is bound to hemoglobin and released in the breath [3, 4]. In 1972, Nikberg et al. [5] were the first to describe exhaled CO (eCO) as a marker to assess different diseases such as cardiovascular diseases, diabetes, and nephritis. Moreover, high levels of eCO have been observed for many diseases [6, 7], such as asthma [8–11] and cystic fibrosis [12, 13], but these findings are still subject of controversy [14].

Many methods have been proposed to measure eCO, such as chemiluminescence [15, 16], gas chromatography [17], and infrared laser spectroscopy [18–21]. In recent years, infrared laser spectroscopy has shown to be a widely used, powerful method for rapid measurement of exhaled breath molecules, suitable for online exhaled breath detection and therefore appears as an emerging technology for medical diagnosis [22, 23]. Major research efforts are directed toward simple, portable sensors with ppbv (parts-per-billion, 1:10^9) sensitivity and subsecond time resolution. For such an approach, continuous-wave quantum cascade lasers (QCL) in combination with absorption spectroscopy are a good choice because QC lasers are compact, have a narrow linewidth and milliWatt power levels in the mid-infrared wavelength region. As CO has its strongest absorptions in this region, it is advantageous to combine such laser sources with optical detection

methods for fast and real-time measurement of trace gases [20, 24, 25].

Considering the breath analysis application of the CO sensor, i.e., concentrations in the ppmv (parts-per-million volume) range and the absorption line strength of the ro-vibrational transition at 4.6 μm (4.5×10^{-19} cm mol^{-1}), two different detection schemes can be considered. A simplified and realistic approach is direct absorption spectroscopy (DAS) [20], as the absorption of 1 ppmv CO is about 0.45 % per meter. With a multipass gas cell of 50 m, 1 ppmv CO will provide about 20 % absorption at 100 mbar. In order to measure lower concentrations, the signal-to-noise ratio can be enhanced by implementing wavelength modulation spectroscopy (WMS) [26].

Alternatively, the sensitivity can be improved by using cavity-enhanced absorption methods, such as cavity ring down spectroscopy (CRDS) [18] and integrated cavity output spectroscopy (ICOS) [27]. CRDS involves coupling the laser beam with a high-finesse optical cavity. This method requires precise alignment and a good mode-matching between the laser frequency and the free spectral range (FSR) of the cavity. Moreover, high-speed electronics and stable optical cavities are required, which is not always appropriate for field applications. On the other hand, ICOS offers long absorption path length without the complexity of active locking [27, 28]. In off-axis ICOS (OA-ICOS), the light is injected into the high fines cavity in such a way that the FSR of the cavity is less than the laser linewidth; as such, many cavity modes couple to the laser light [29, 30]. In such a setup, the alignment is robust as the laser beam does not optically require strong mode-matching to the cavity. For breath analysis purpose, the use of moderate reflective mirrors is sufficient, reducing the difficulty of the optical alignment.

In this paper, we propose both detection schemes and present their different features such as detection limit, stability, and reproducibility. The sensors have been validated with online measurements of exhaled human breath.

2 Experimental details

2.1 Sensors setup

The laser source is a continuous-wave distributed feedback QC laser (M905I, Maxion Technologies) operating at a center wavelength of 4.61 μm (2169.2 cm^{-1}). As the CO sensor is intended to monitor eCO concentrations, the wavelength is chosen to minimize the spectroscopic interference effects of H_2O and CO_2, present in the exhaled breath at about 2 and 5 % levels, respectively. Figure 1 shows the absorption coefficient profiles at 100 mbar of the CO R(6) absorption line at a 10 ppbv volume mixing ratio

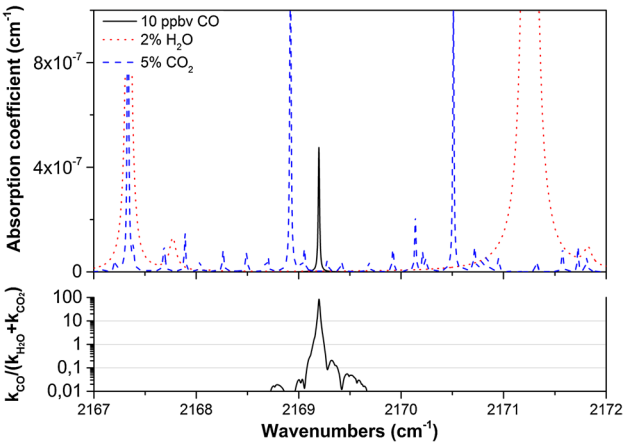

Fig. 1 Simulated spectra based on HITRAN 2008 database [31] for 10 ppbv CO (*black solid line*), 2 % water (*red dotted line*), and 5 % CO_2 (*blue dashed line*) in the spectral range of 2167–2172 cm^{-1} at 100 mbar. The *lower panel* is the ratio of the absorption coefficient of CO with the two other interfering gases. A maximum of 84 is reached

in the presence of 2 % water and 5 % CO_2 (based on the HITRAN database [31]). This absorption of CO is up to 84 times stronger than the background, coming from the tail of a neighboring H_2O line.

The laser is incorporated in a laser housing (LDM-4872, ILX Lightwave), which has been modified replacing the water cooling system by an air cooling system. The stable temperature of the laser at +33 °C is achieved with a thermoelectric Peltier element and a temperature controller (LDT-5980, ILX Lightwave). With a supply current of 450 mA, the laser output power is about 20 mW.

The two optical schemes, used in this research, are depicted in Fig. 2. In both cases, the laser beam is collimated with an aspherical lens ($f = 4$ mm, NA = 0.56), which is incorporated in the laser housing. With a beam splitter (ratio 60:40), 60 % of the light is used either for wavelength modulation spectroscopy or OA-ICOS, the remaining part of the light goes to a reference CO gas cell.

For wavelength modulation spectroscopy (Fig. 2a), the light from the beam splitter passes through a 20-cm-long absorption gas cell. The 35-ml volume gas cell is made of a glass tube with an inner diameter of 1.5 cm and two ZnSe windows at Brewster angle to minimize optical interferences and maximize the transmission of the linearly polarized light of the QCL. The pressure of the gas in the cell is maintained at 100 mbar, and a continuous flow of 2 l h^{-1} is set by using mass flow controllers (Brooks Instrument). Finally, the optical beam is focused ($f = 5$ cm) onto a room-temperature photovoltaic detector (PV-5, VIGO, response time 20 ns, detectivity ~8×10^8 cm Hz$^{1/2}$ W^{-1}). The electronic signal from the detector is sent to two lock-in amplifiers (Stanford Research System SR844) to retrieve the 1f and 2f harmonic signals. The 1f signal is

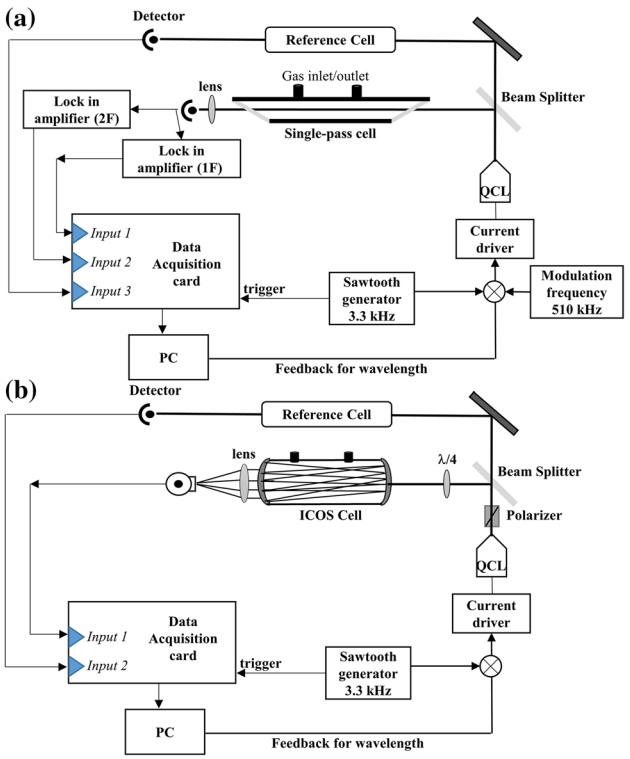

Fig. 2 General scheme of the experimental setup for detecting CO with two spectroscopy methods. **a** The QCL is sent through a single-pass cell. The output signal from the room-temperature photovoltaic detector is sent to lock-in amplifiers to separate the second and first harmonics. **b** The QCL beam is sent off-axis to the OA-ICOS cell. A polarizer and a quarter wave plate are used to reduce optical feedback noise. The transmitted beam from the OA-ICOS cell is focused onto a Peltier-cooled photovoltaic detector. In both schemes, output signals are analyzed by a LabVIEW program. Laser locking is accomplished by scanning a reference CO gas, generating an error signal correcting the DC current of the laser

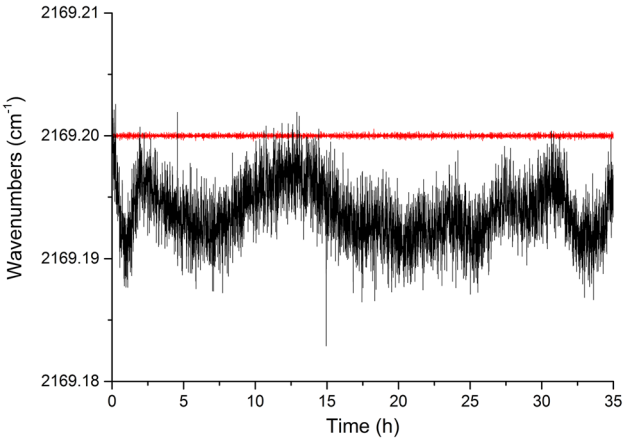

Fig. 3 Fluctuations of the laser wavelength over time when the laser frequency is free running (*black line*) or when the laser wavelength emission is locked at the center of CO absorption line (*red line*)

used to measure the laser power fluctuations and to normalize the 2f signal [32]. Electronically, the laser driver (LDX-3232, ILX Lightwave) is externally modulated at two different frequencies. Firstly, a sine wave modulation (510 kHz) is applied to the laser current to generate the wavelength modulation signal. The amplitude modulation is about 0.1 % of the DC laser current. The second modulation (3.3 kHz) has a sawtooth waveform. This sawtooth has an amplitude of 0.6 % of the DC laser current, such that the wavelength of the laser is scanned over the absorption line of CO.

For OA-ICOS spectroscopy (Fig. 2b), a Rochon polarizer (MgF_2 Prisms, extinction ratio 10^{-5}) and a quarter wave plate (zeroth order, Altechna) are added before the gas cell to minimize optical feedback into the laser. The gas cell is a 15-cm stainless steel tube (inner diameter 2 cm, volume 47 ml). The pressure inside the cell is maintained at 20 mbar, and the gas flow is set to 2 l h^{-1}. The two optical mirrors of the cell, forming the optical resonator, have a radius of curvature of 1 m and a reflectivity of 99.7 % at 4.61 µm. The finesse of such optical resonator, or path enhancement, is about 1050, and therefore, the effective optical path is about 160 m. The light transmitted through the cell is collected and focused via a plano-convex lens ($f = 5$ cm) onto a Peltier-cooled photovoltaic detector (PVI-4TE-5, VIGO, response time 20 ns, detectivity ~3 × 10^{11} cm $Hz^{1/2}$ W^{-1}). In the case of OA-ICOS, the only modulation applied to the laser current is the sawtooth waveform, used to scan the wavelength over the CO absorption line.

Most of the time, QCL-based sensors are exposed to drifts of the laser wavelength, which has impact on the long-term stability of the system. In order to improve the performance of the CO sensors, the QCL frequency is locked to the scanned CO absorption line, using a 10-cm-long reference cell containing 0.1 % CO in N_2 at 100 mbar. About 6 mW of laser power goes through the reference cell onto a room-temperature photovoltaic detector (PV-5, VIGO). The signal of the detector is used in a feedback loop to keep the CO absorption line in the middle of the scanned wavelength range. For each scan of the laser wavelength, a LabVIEW program finds the minimum position on the absorption line. An error signal is generated that adjusts the DC current of the laser driver. Figure 3 shows the wavelength stability of the laser in unlocked and locked cases together with the corresponding error signal. The system is staying locked over days. The laser system is placed in an aluminum transport box (footprint 55 × 35 × 35 cm^3), and the temperature inside the box is kept stable by a temperature controller and heating resistors, the latter mounted on the optical breadboard of the sensor.

2.2 Concentration measurements

Prior to each experiment, the gas sensor is calibrated with a mixture of 1 ppmv of CO in N_2 (calibration mixture, Linde, the Netherlands) and hydrocarbon-free air used as a background reference gas. These two gas mixtures are used as references to determine unknown CO concentrations. A single measurement consists of scanning the laser over the spectral region of the CO absorption line, typically from 2169.16 to 2169.24 cm^{-1} and making a linear fit of the signal with the 1 ppmv reference mixture (both background subtracted). Assuming weak absorption, the unknown concentration is retrieved by multiplying the reference CO concentration by the first-order coefficient of the linear fit. An example is given in Fig. 4, in the case of an eCO measurement.

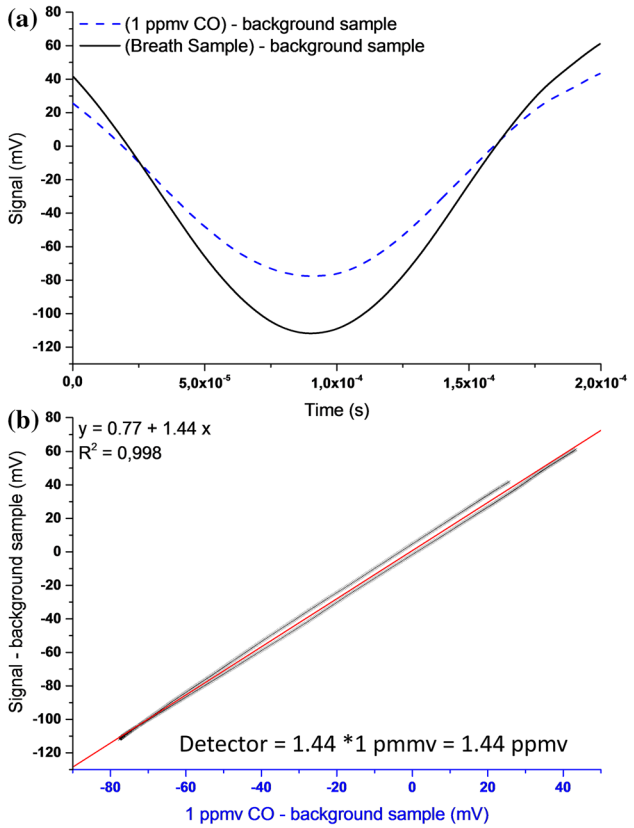

Fig. 4 Steps to measure an unknown CO concentration. **a** Previous to the experiment, the scans from a 1 ppmv CO mixture and the background sample are recorded (not shown). The subtractions of both scans results in a reference scan (*blue dash line*). The signal of an unknown mixture (here a breath sample) is acquired, and the recorded background scan is subtracted (*black line*). **b** Assuming a linear response of the system, the CO concentration of the breath sample is calculated from the slope value (**a**) of a linear fit between the reference scan and the scan of the sample shown in **a** ($Sample_{scan} - background_{scan}$) = 1.44 × ($1ppmCO_{scan} - background_{scan}$) + 0.77

The weak absorption approximation is totally appropriate for the WMS setup; however, for the same gas concentration, this assumption is wrong in the case of OA-ICOS, as the effective optical path length is enhanced to produce detectable absorption. The result is a nonlinear response of the system, which eventually can be corrected by data processing. More details on this are presented in paragraph 3.1.

2.3 Online breath sampling

A custom-built breath-collection device, as described previously [33], is used for online exhaled breath measurements. Briefly, the design of the device is following the recommendations of the American Thoracic Guidelines for collecting exhaled NO [34]. It consists of a mouthpiece, a pressure meter, and, to establish an exhaled flow resistance, a Teflon stopper with a precise hole, followed by a Teflon tubing connected to the gas inlet of the optical sensor. The subjects exhale through the mouthpiece at constant flow rate by maintaining a constant mouth pressure (induced by the Teflon stopper). As CO molecules are also produced by the nose [35], the overpressure is set to 10 mbar to prevent nasal contamination. To help the patient maintaining a constant exhalation flow rate, three LEDs on the pressure meter indicates to increase, decrease, or maintain the exhalation flow. By changing the size of the hole in the Teflon stopper, various exhalation flow rates can be collected from the subjects. The breath sampler was calibrated for each Teflon resistance piece with a mass flow meter (Brooks Instrument, max flow: 5 l h^{-1}, accuracy ±1 %), ranging from 0 to 30 l min^{-1}. This custom-built breath-collection device is connected directly to the QCL sensor by ¼-inch Teflon (PTFE) tubing.

3 Results

3.1 Characteristics of QCL sensor

CO samples are measured over time to evaluate the features of the two sensors, such as detection limit, calibration curve, saturation, and reproducibility.

The detection limit and fluctuations of the sensors' signals are evaluated by measuring, after calibration, the concentration of the hydrocarbon-free air over hours and calculating the Allan variance for different time periods.

For the WMS setup, a detection limit of 7.1 ppbv CO in 1 s is achieved. As shown by the Allan variance plot (Fig. 5a, black line), the precision of the measurements can be improved to 2.1 ppbv by averaging the signal over 300 s. Several measurements with the same 1 ppmv CO mixture

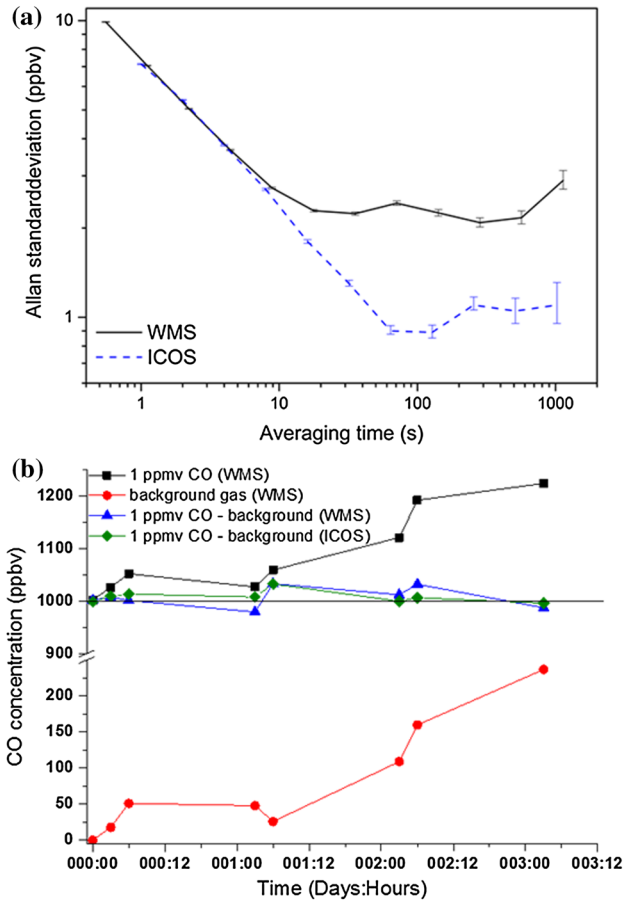

Fig. 5 **a** Allan deviation of the WMS and OA-ICOS setups, showing the precision on CO measurements as a function of integration time of the signal. Both following a similar trend at short integration time (7 ppbv at 1-s integration time), the OA-ICOS setup reaches sub-ppbv precision with an integration time of about 100 s. **b** Long-term measurements with the WMS setup, or reproducibility, of a 1 ppmv CO mixture and background gas. If both measurements of the background and the CO mixture are changing over time, the difference is staying within ±40 ppbv. Similar performance has been observed with the ICOS setup

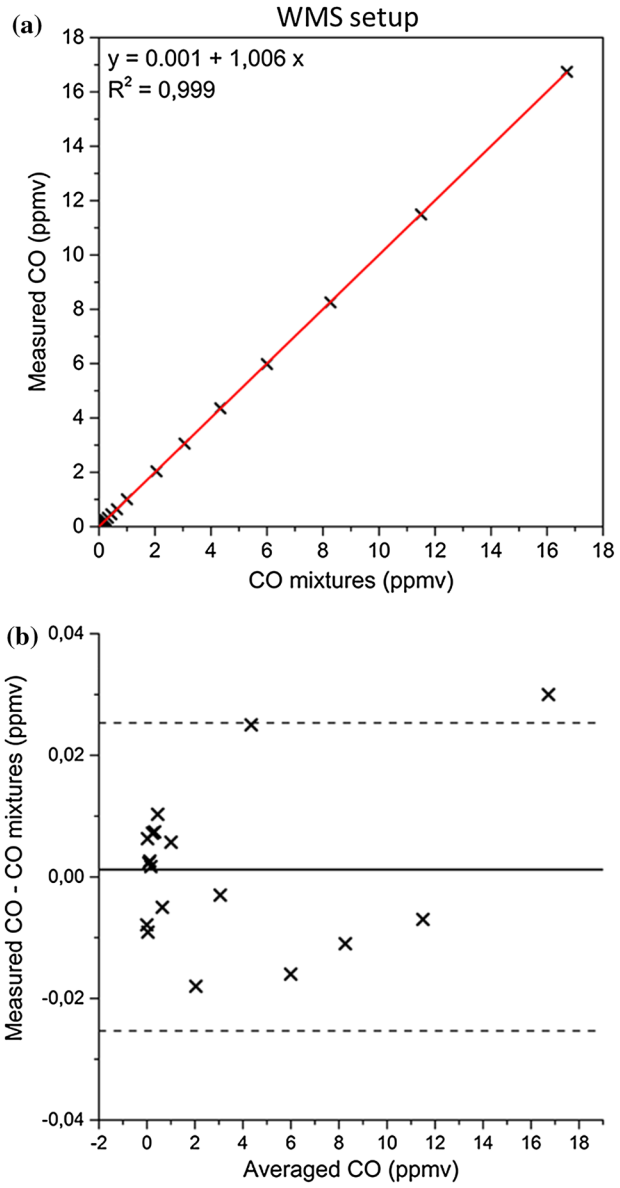

Fig. 6 **a** Linearity of the WMS-2f/1f setup. Measured CO concentration versus prepared dilutions of standard calibration mixture of 1 ppmv CO in N_2. **b** Residual. The *black line* indicates the average deviation of the measurements with the fit (1.2 ppbv), the *dash lines* ×2 the standard deviation of them (STD = 13 ppbv)

have been taken over a time period of 3 days (Fig. 5b). During this period, the background signal and the 1 ppmv signal are changing significantly (>200 ppbv); however, the difference between the 1 ppmv CO signal and the background signal stays within 40 ppbv.

For OA-ICOS, a similar detection limit of 7 ppbv of CO in air within 1 s is achieved. The Allan variance (Fig. 5a, dashed blue line) indicates the possibility to improve the precision of the measurements to 0.89 ppbv with an integration time of 128 s. Concerning the long-term measurements over 3 days, a similar behavior as with WMS is observed with OA-ICOS (Fig. 5b).

The linear response to different CO concentrations for both systems is tested, and the results are displayed in Figs. 6 and 7 for the WMS and OA-ICOS setup, respectively. The different CO mixtures are prepared from a 20-ppmv CO gas bottle and hydrocarbon-free air; the dilution is achieved by using dynamic mixing with two mass flow controllers.

For the WMS setup, the sensor shows a good linearity with the different CO mixtures. The linear fit of the data has a slope value close to 1 (1.006) and an offset of 1 ppbv. The residual, Fig. 6b, is within the detection limit of the signal and does not show particular trend. Measurement of pure CO indicates a saturation around 40 ppmv, due to

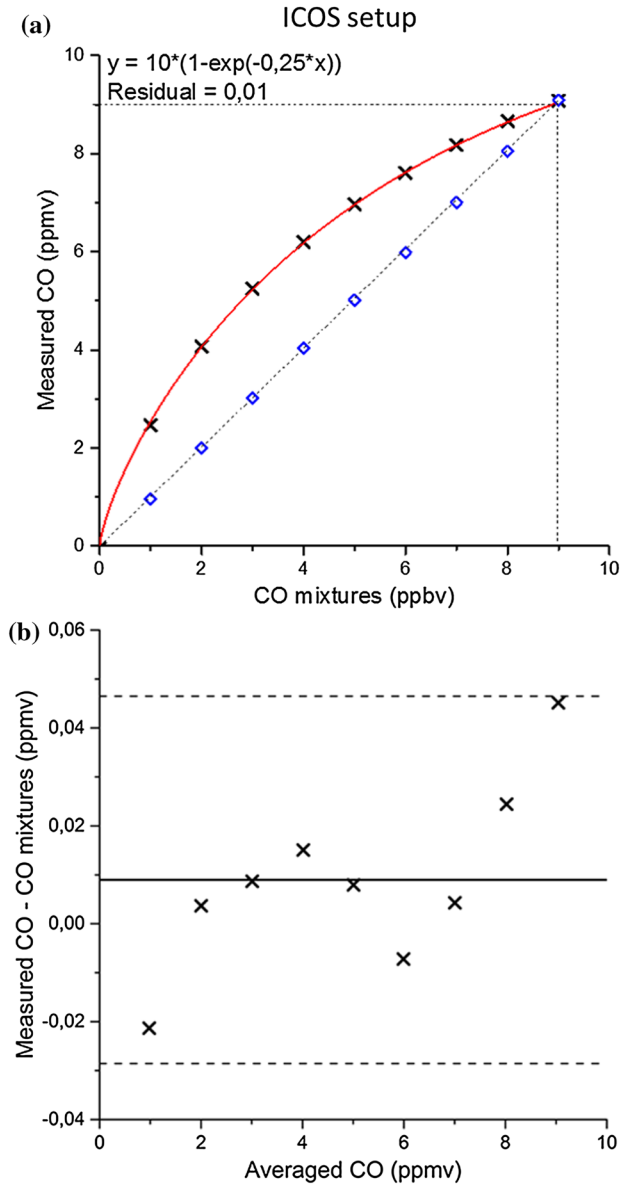

Fig. 7 **a** Linearity of the OA-ICOS setup. Measured CO concentration versus prepared dilutions of a mixture of 9 ppmv CO in N_2. **b** Residual. The *black line* indicates the average deviation of the measurements with the fit (9 ppbv), the *dash lines* two times the standard deviation of them (STD = 19 ppbv)

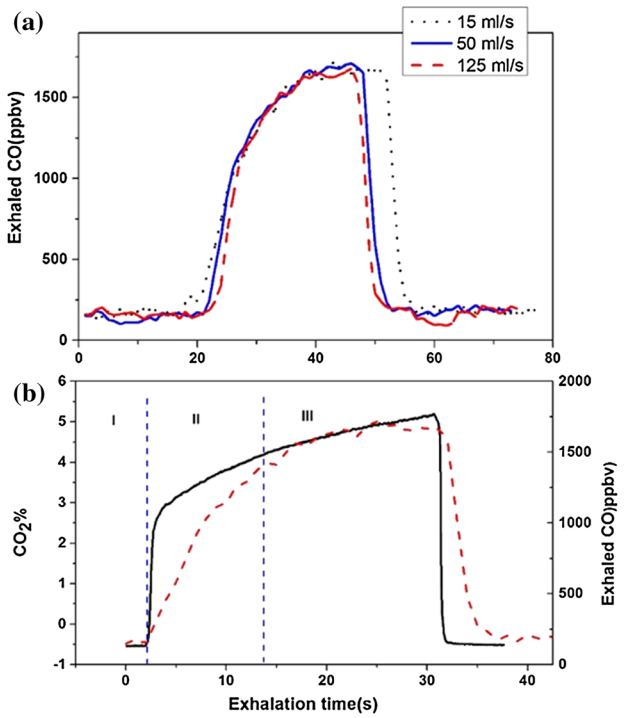

Fig. 8 **a** Recorded exhaled CO levels using OA-ICOS during online sampling from a single exhalation at different flow rates. **b** Real-time measurements of CO (*red dashed line*, QCL-based sensor) and CO_2 profiles (*black solid line*, Loccioni breath sampler) during a single exhalation. Phase I shows the initial stage of expiration, phase II shows a sharp rising of waveform slope, phase III represents alveolar plateau

the dynamic range of the settings of the lock-in amplifier. However, this limitation can be removed by decreasing its input gain.

For the OA-ICOS setup, the sensor does not provide a linear response because of the strong CO absorption and an absorption path length of 160 m inside the gas cell. To reduce this effect, the pressure of the gas cell is set to 20 mbar. At this pressure, 1 ppmv CO mixture induces an absorption of about 26 % of the incident light. Concentrations higher than 10 ppmv are not quantifiable due to the saturation of the system. Figure 7a (calibration done with a 9 ppbv CO mixture in N_2) shows an exponential behavior of the measured concentrations versus the different CO mixtures, following the Beer–Lambert law. By implementing in the data processing software the parameters of the exponential fit, the response could be made linearly. Figure 7b displays the residual of the linear fit after correction by the software.

3.2 CO: flow dependency and breath-holding

For a reliable analysis, standardization of the measurements is needed; also to be able to compare different sampling methods. For this, the flow rate dependence of eCO concentrations and the effect of breath-holding are studied. The dependence of the eCO concentration on exhalation flow rates is tested on nine healthy volunteers (25 ± 5 years). Subjects inhaled through their nose and exhaled immediately into the device (which is connected to the sensor) at three different expiratory flow rates (15, 50, 125 ml/s, Fig. 8a). A typical expiratory CO plateau (Fig. 8b) is observed with three phases, which are similar to a CO_2 expirogram; for measuring the CO_2 concentrations,

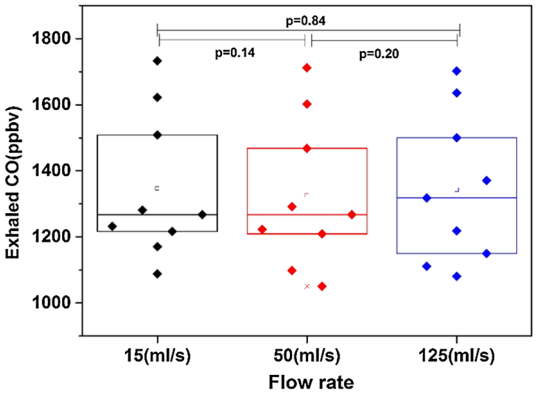

Fig. 9 *Box Plot* shows distribution of exhalation data of nine individuals (*diamonds*) for three different flow rates (15, 50, and 125 ml/s). The *p* values show that there is no difference in eCO levels for the different flow rates

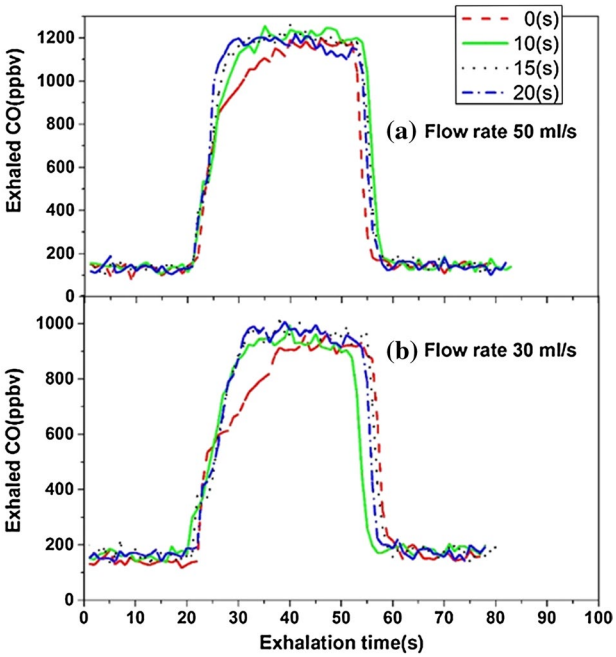

Fig. 10 Online exhaled CO concentrations are shown for various breath-holding times (0, 10, 15, 20 s), measured with WMS. **a** Exhalation flow rate 50 ml/s, **b** 30 ml/s. If almost similar plateau levels are reached, the longer the breath-holding the faster they are reached

a commercially breath sampler (Loccioni, Italy) was used. Phase I represents the exhaled breath from the conducting airways (dead space) in the initial stage of expiration, phase II represents the exhaled breath from the terminal airways and the alveoli with the shortest transit times, and phase III reflects the gas being exhaled from the rest of the alveoli (alveolar plateau). The CO concentration is determined by averaging the plateau level in phase III. The highest possible flow, at which a constant flow rate is maintained long enough to obtain a reliable CO plateau, was 125 ml/s. The effect of the exhalation flow rate on the CO concentration is analyzed using a paired *t* tests (Fig. 9). Significance is defined as a *p* value of <0.05. It is found that there is no significant difference between the assessed flow rates.

The breath-holding maneuver is done by asking subjects to hold their breaths for various time periods and then exhaled online in the device. We used flow rates of 30 and 50 ml/s. By increasing the breath-holding time, a steeper slope is observed within phase II and the plateau level appears sooner (Fig. 10). The average CO concentration of the plateau level increases slightly with increasing breath-holding period. Since the CO level in the blood is not in equilibrium with the lungs, there will be a continuous emission rate into the lungs, resulting in an increasing plateau level.

4 Discussion

Two detection schemes, based on OA-ICOS and WMS, have been implemented and tested in order to develop a CO sensor for real-time measurements of exhaled CO in human breath. For healthy subjects, exhibiting CO levels of few ppmv, both schemes demonstrate a high reproducibility and enough sensitivity for online measurements of exhaled human breath. Both systems show very similar performance, have a compact design, with a simple and robust optical alignment, and appear adequate for applications in a clinical environment.

The noise-equivalent detection limit at 1-s averaging is about 7 ppbv for both OA-ICOS and WMS sensors. It is interesting to notice that a similar sensitivity have been reached, although the detection systems are different. In the case of WMS, the optical transmission of the gas cell is close to 100 %, as the windows are at Brewster angle and the laser light is linearly polarized. The room-temperature infrared detector is sufficient to generate an appropriate signal of hundreds of millivolts. On the other hand, the weak absorption due to the single-pass cell arrangement needs to be detected with a lock-in amplifier. In the case of OA-ICOS, only few microwatts can reach the detector, as a consequence of the high reflectivity of the cell's mirrors and the off-axis alignment. As such, a 4-stage cooled infrared detector is needed, offering a 400 times better detectivity as compared to the room-temperature WMS detector, to get only a few millivolts signal.

Both detection systems are using the same feedback to stabilize the laser wavelength, and in the case of WMS, the 1f signal proportional to the laser intensity is used to normalize the 2f signal. The long-term stabilities of the systems are almost identical even though the OA-ICOS system has a slightly better stability. As the WMS absorption is

weaker as compared to the OA-ICOS (1 ppmv CO induces an absorption of 0.09 % for WMS and 50 % for ICOS), WMS signal is consequently more sensitive to residual optical fringes, originating from the collimation lens, focus lens, and cell windows. Thermal isolation of the optical setup in an aluminum box, combined with a temperature control system, makes both sensors almost identical in terms of long-term stability.

The response time and sampling frequency of both systems are very similar and sufficient for online eCO measurements as shown in Fig. 8. The small volume of the cells, the low pressure of the gas, and the moderate flow rate through the gas cell of 2 l h^{-1} are leading to a response of less than 10 s. In the case of eCO measurements, this could easily be adapted and improved as the recommended exhaled breath flow rate is at 180 l h^{-1} (50 ml s^{-1}).

OA-ICOS suffers from a strong limitation, due to the saturation of the absorption signal (Fig. 7a), and CO concentrations over 10 ppmv cannot be measured accurately. This limitation can be reduced by decreasing the reflectivity of the mirrors until the intensity noise of the source or the detector noise starts to dominate the absorption signal. However, the response of the system can be measured and corrected, to appear linearly. The WMS sensor does not suffer from a nonlinear response. A saturation appears around 40 ppmv due to the limitations of the dynamic range of the lock-in amplifier. A simple change in the gain of the lock-in amplifier allows to measure higher concentrations. In the case of our 20-cm-long gas cell, the optical signal saturates for CO concentrations higher than 0.1 %. Compared to the OA-ICOS, the WMS setup is more appropriate for measurements in a wide range of concentrations.

In comparison with previous reported works, the OA-ICOS method demonstrates a similar sensitivity as reported by Fritsch et al. [18] where a CRDS setup based on a tunable side band laser showed a detection limit of 7 ppb $Hz^{-1/2}$ of ^{13}CO in breath. However, OA-ICOS is known to be less sensitive to optical alignment and therefore more suitable for a mobile, transportable sensor. Interestingly, the WMS sensor shows the similar detection limit and appears to be a simpler setup and straightforward to assemble, as the single-pass cell does not require any optical alignment. The fast frequency modulation is easily handled by the QCL, and the demodulation detection scheme can be miniaturized if the electronics is specifically designed for this application. However, the sensor is more sensitive to residual optical interferences, and special care should be taken for AR-coating all the optical elements at the specific laser wavelength.

In addition, the effect of exhaled flow rates on CO concentration levels was studied. It was found that exhaled CO levels were not affected by different exhalation flow rates. As the central airway is an important factor determining flow dependency [14], this strongly indicates that there is no contribution of CO from airway epithelium, so the origin of CO is from the alveoli. Support for this is also given by the increase in eCO concentrations after breath-holding; with 10-s breath hold, an eCO increase of up to 20 % is observed, while collecting the breath in bags. During this breath-holding period, diffusion of CO into the alveoli occurs and affects the concentration of CO in exhaled breath. The significant increase during breath-holding supports the idea that CO has no airway origin as suggested by nonsignificant flow dependency. As a result, using bags to collect the breath remains difficult as breath-holding maneuver is influencing the collected eCO concentrations.

Acknowledgments This work was supported by the European Regional Development Fund, province of Gelderland, GO-EFRO Project (No. 2009-010034), and a visiting scholarship from the Research and Technology of the Islamic Republic of Iran.

References

1. R. Tenhunen, H.S. Marver, R. Schmid, Proc. Natl. Acad. Sci. USA **61**(2), 748–755 (1968)
2. R.F. Coburn, R.E. Forster, W.J. Williams, J. Clin. Investig. **43**(6), 1098–1103 (1964)
3. L. Wu, R. Wang, Pharmacol. Rev. **57**(4), 585–630 (2005)
4. M.G. Zhou, Y. Liu, Y.X. Duan, Clin. Chim. Acta **413**(21–22), 1770–1780 (2012)
5. I. Nikberg, V. Murashko, I. Leonenko, Vrachebnoe delo **12**, 112 (1972)
6. S.W. Ryter, J.M. Sethi, J. Breath Res. **1**(2), 026004 (2007)
7. B. Antus, I. Horvath, J. Breath Res. **1**(2), 024002 (2007)
8. K. Zayasu et al., Am. J. Respir. Crit. Care Med. **156**(4), 1140–1143 (1997)
9. I. Horváth et al., Thorax **53**(8), 668–672 (1998)
10. C.G. Uasuf et al., J. Pediatr. **135**(5), 569–574 (1999)
11. M. Yamaya et al., Clin. Exp. Allergy **31**(3), 417–422 (2001)
12. P. Paredi et al., Thorax **54**(10), 917–920 (1999)
13. J.D. Antuni et al., Thorax **55**(2), 138–142 (2000)
14. W. Zetterquist et al., Eur. Respir. J. **20**(1), 92–99 (2002)
15. H. Vreman et al., Clin. Chem. **42**(1), 50–56 (1996)
16. C. Zhuang, W.J. Buttner, J.R. Stetter, Electroanalysis **4**(3), 253–266 (1992)
17. W. Miekisch, J.K. Schubert, G.F.E. Noeldge-Schomburg, Clin. Chim. Acta **347**(1–2), 25–39 (2004)
18. T. Fritsch, P. Hering, M. Mürtz, J. Breath Res. **1**(1), 014002 (2007)
19. M.R. McCurdy et al., J. Breath Res. **1**(1), 014001 (2007)
20. J.H. Shorter et al., IEEE Sens. J. **10**(1), 76–84 (2010)
21. B.W.M. Moeskops et al., Appl. Phys. B-Lasers Opt. **82**(4), 649–654 (2006)
22. J.H. Shorter et al., J. Breath Res. **5**(3), 037108 (2011)

23. M. Sowa, M. Murtz, P. Hering, J. Breath Res. **4**(4), 047101 (2010)
24. S.-S. Kim et al., IEEE Sens. J. **10**(1), 145–158 (2010)
25. A.A. Kosterev, IEEE J. Quantum Electron. **38**(6), 582–591 (2002)
26. R. Kormann et al., Rev. Sci. Instrum. **76**(7), 075102 (2005)
27. G.S. Engel et al., Appl. Opt. **45**(36), 9221–9229 (2006)
28. A. O'Keefe, Chem. Phys. Lett. **293**(5), 331–336 (1998)
29. E.J. Moyer et al., Appl. Phys. B-Lasers Opt. **92**(3), 467–474 (2008)
30. D.D. Arslanov, S.M. Cristescu, F.J.M. Harren, Opt. Lett. **35**(19), 3300–3302 (2010)
31. L.S. Rothman et al., J. Quant. Spectrosc. Radiat. Transf. **110**(9), 533–572 (2009)
32. G.B. Rieker, J.B. Jeffries, R.K. Hanson, Appl. Opt. **48**(29), 5546–5560 (2009)
33. S. Cristescu et al., Appl. Phys. B **110**(2), 203–211 (2013)
34. P.E. Silkoff, Chest **126**, 1013–1014 (2004)
35. J.A. Andersson, R. Uddman, L.O. Cardell, J. Allergy Clin. Immunol. **105**(2), 269–273 (2000)